Research Article Vol. 16, No. 6 / 1 Jun 2026 / Optical Materials Express 1760
Optical Materials EXPRESS

Stereolithography 3D printing of a cyclic olefin resin for terahertz quasi-optical applications

Luke Phillips,[1,*] Sanchit Kondawar,[2,3] Harry J. Godden,[2] Ben Douglas,[4] Nathan R. Fox,[2] Mohammed Salih,[2] Alexander Valavanis,[2] Andrew D. Burnett,[5] Robert Kay,[1] Raymond A. Weitekamp,[6] and Ehab Saleh[1,7]

[1]School of Mechanical Engineering, The University of Leeds, Leeds LS2 9JT, UK
[2]School of Electronic and Electrical Engineering, The University of Leeds, Leeds LS2 9JT, UK
[3]UCL Electronic & Electrical Engineering, Roberts Building, Torrington Pl, London WC1E 7JE, UK
[4]School of Chemical and Process Engineering, University of Leeds, Leeds, UK
[5]School of Chemistry, The University of Leeds, Leeds LS2 9JT, UK
[6]polySpectra, Berkley, California, 9470, USA
[7]College of Engineering and Technology, University of Doha for Science and Technology, Doha, Qatar
*mnlcjp@leeds.ac.uk

Abstract: Stereolithography (SLA) additive manufacturing (AM) is an emerging technique for fabricating terahertz (THz) complex quasi-optical components at low-cost. However, most photopolymers exhibit significant absorption losses, limiting the performance of SLA-produced quasi-optics. Cyclic Olefin Resin (COR) was identified as a promising alternative owing to its formulation of olefinic monomers highly transparent to THz radiation. SLA-fabricated COR samples were characterized from 0.5 to 6 THz using time-domain spectroscopy. Gyroid lattices were printed to assess the feasibility of sub-wavelength features at 1 THz. Additionally, plano-convex and Fresnel lenses were manufactured and evaluated using a THz quantum cascade laser (QCL) system. COR exhibited an absorption coefficient of (3.96 ± 0.01) cm^{-1} at 1 THz, increasing to (11.29 ± 0.39) cm^{-1} at 6 THz, substantially lower than conventional photopolymers, which exceed 60 cm^{-1} at 2 THz. Gyroid lattices demonstrated reproducible features, while the lenses operated efficiently at 3.4 THz. COR was shown to be considerably more transparent to THz radiation than standard photopolymers, enabling the fabrication of efficient quasi-optics using low-cost SLA systems, improving accessibility of bespoke THz optical components.

Published by Optica Publishing Group under the terms of the Creative Commons Attribution 4.0 License. Further distribution of this work must maintain attribution to the author(s) and the published article's title, journal citation, and DOI.

1. Introduction

The terahertz (THz) region of the electromagnetic spectrum encompasses frequencies from 0.1 to 10 THz, with corresponding wavelengths (λ) ranging from 3 mm to 30 µm [1]. A key characteristic of THz waves is the ability to penetrate a range of materials, including polymers, textiles, and other non-polar materials [2]. Additionally, the radiation is non-ionizing [3]. These properties are desirable for a range of application fields, including material characterization, medical imaging, security screening and quality control [4,5].

Key components in THz systems are quasi-optics, such as THz lenses, which play a crucial role in manipulating and directing THz radiation. Conventional fabrication methods for these lenses include molding, subtractive manufacturing and powder-compression techniques [6–8], while lithographic and etching processes are also used for producing high-resolution patterned structures [9]. However, these processing routes typically impose design restrictions and are limited by their achievable resolution and material compatibility, thereby restricting the range and availability of quasi-optical components [10]. As a result, commercially available THz optics are

#601125 https://doi.org/10.1364/OME.601125
Journal © 2026 Received 8 Apr 2026; revised 14 May 2026; accepted 15 May 2026; published 21 May 2026

Optical Materials EXPRESS

costly, with specialized or complex designs often being unavailable or prohibitively expensive due to the increased fabrication difficulty.

Additive Manufacturing (AM) has emerged as a promising method for fabricating THz quasi-optical components, enabling the manufacture of low-cost, complex designs with increased design flexibility [11–13]. A range of quasi-optical components have been manufactured via AM, including lenses, filters and waveguides [14–16]. The localized production and cost reduction of AM-produced quasi-optics has the potential to significantly improve the accessibility of THz systems for both research and industrial applications.

However, a crucial requirement for quasi-optics is that the surface roughness and geometric features of printed components must be considerably smaller than the operating wavelength to minimize scattering and attenuation [15]. A recent review by Phillips et al. (2025) highlights that Vat Photopolymerization (VP) techniques, including Stereolithography (SLA), can produce optically smooth surfaces and geometric features with dimensions on the order of the wavelength scale for 1 to 10 THz (300 µm to 30 µm) [17]. The review showed that VP techniques can achieve feature sizes as small as 15 µm and surface roughness average (Ra) values below 5 µm.

Despite their advantages, SLA processes are limited by the optical properties of photopolymer feedstock materials at THz frequencies. Duangrit et al. (2019) found that the absorption coefficient of commercially available AM photopolymers ranges from 19–27 cm^{-1} at 1 THz [18]. Additionally, Phillips et al. (2024) and Brodie et al. (2022) reported a significant increase in the absorption coefficients at higher frequencies, reaching approximately 60 cm^{-1} at 2 THz [19,20]. In contrast, polymers conventionally molded into THz lenses, such as Polytetrafluoroethylene (PTFE) and TPX^{TM}/ Polymethylpentene (PMP), typically have absorption coefficients below 3 cm^{-1} at 1 THz [21,22]. Consequently, SLA-produced quasi-optics would either be extremely lossy, owing to the elevated absorption coefficients of photopolymers, or would be restricted to very thin designs to minimize losses. For example, photopolymer plano-convex lenses are typically limited to focal lengths above 100 mm, since shorter focal lengths require increased thickness, which results in greater absorption losses.

A Cyclic Olefin Resin (COR) was identified as a promising solution to address the optical limitations of conventional photopolymers. The formulation of the COR included olefinic monomers, which upon exposure to light underwent crosslinking, initiated by a ruthenium-based catalyst. The formulation of COR was encouraging, as prior research had demonstrated that polyolefins, Polypropylene (PP) and TPX/PMP, exhibited high transparency to THz radiation, with them being widely used as THz lenses and windows [23–25]. Therefore, a photopolymer containing olefinic monomers could offer increased transparency to THz radiation. Additionally, as the catalyst was activated when exposed to 405 nm light it ensured compatibility with a range of low-cost SLA printers.

Several studies have recognized the potential of Cyclic Olefin Copolymers (COC) for additive manufacturing of quasi-optics [12,26,27], with COR designed to mimic the properties of COC. COC is commercially available in filament form (TOPAS) and is compatible with a range of material extrusion AM systems. However, extrusion-based AM processes often produce features with lower resolution and rougher surfaces than SLA. No literature could be found characterizing the optical properties of a COR compatible with SLA systems.

In this study, COR samples, including characterization disks and gyroid lattices were fabricated using an SLA-printing process to enable optical characterization at THz frequencies via THz time-domain spectroscopy (THz-TDS) and geometric inspection of the SLA process resolution. The goal was to determine whether COR exhibited high transparency to THz radiation and could be processed via SLA to achieve high-resolution features. Subsequently, quasi-optical components were fabricated from COR and assessed using a THz quantum cascade (QCL) system to validate their performance.

Optical Materials EXPRESS

2. Methodology

2.1. Material

The resin selected for this study was COR Alpha, developed by polySpectra. It was chosen for its compatibility with low-cost SLA printers using a 405 nm light source. The COR Alpha formulation consists of olefinic monomers, predominantly dicyclopentadiene and tricyclopentadiene, as well as a light-activated ruthenium catalyst and functional additives. When exposed to ultraviolet light, the ruthenium catalyst activates, reacting with surrounding olefin monomers, triggering localized Ring Opening Metathesis Polymerization and cross-linking within the material (see Fig. 1). This chemical process is known as Photolithographic Olefin Metathesis Polymerization (PLOMP) [28].

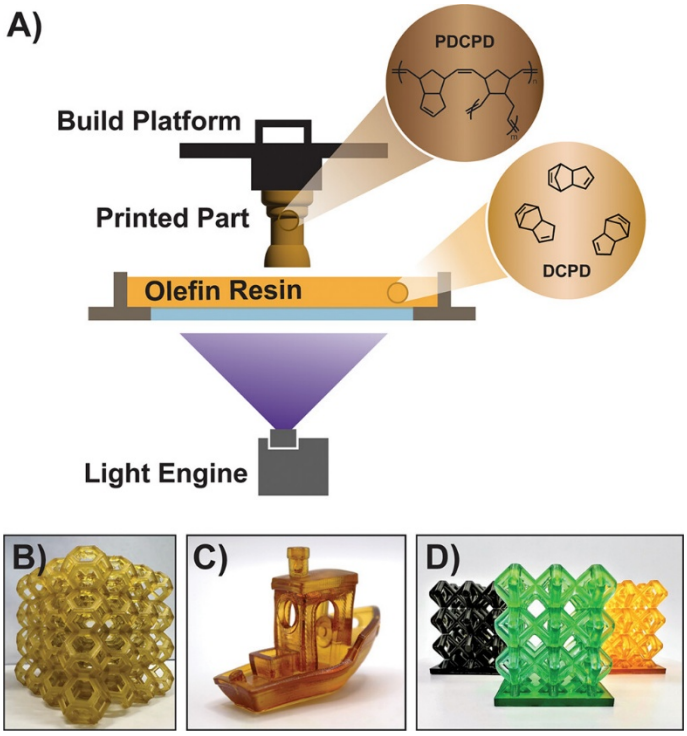

Fig. 1. Photoactivation of olefin metathesis reactions enables AM of olefin resins. (A) Schematic of the SLA printing process using an olefin resin. (B-D) Examples of printed components produced from dicyclopentadiene (DCPD) based olefin-resins utilizing resins from (B) Promerus, (C) Leguizamon et al., [29] and (D) polySpectra. Reproduced under terms of the CC-BY-NC-ND 4.0 license. Copyright © 2024, Greenlee et al. Published by American Chemical Society. [30].

For comparison, AM photopolymers are typically composed of acrylic monomers and oligomers, alongside photoradical initiators. When exposed to UV light, the photoinitiators decompose, generating free radicals. These radicals initiate polymerization by reacting with monomers and oligomers to form polymer chains, which then cross-link to form a polymer network [31]. Typically, acrylate, methacrylate, epoxy and vinyl monomers are used [32,33], which have different chemical, mechanical, and dielectric properties than the COR materials. In the context of dielectric properties, the lack of any heteroatoms in the COR polymer network contributes to the low loss when compared to traditional systems.

Optical Materials EXPRESS

COR Alpha was purchased directly from polySpectra and stored in an industrial freezer at -20°C when not in use, to prolong its shelf life.

2.2. Sample designs

A disk with a diameter of 25.4 mm and a thickness of 2 mm was modelled using Autodesk Fusion 360. The diameter was selected to ensure the sample was compatible with existing THz-TDS sample mounts. The chosen thickness was balanced to allow large enough transmission of THz radiation to enable measurements across a wide bandwidth, while also providing sufficient strength to minimize the risk of thermal defects during post-processing stages.

To determine if sub-wavelength geometric features at 1 THz ($\lambda = \sim 300$ µm) could be successfully and repeatably manufactured from COR using SLA, two gyroid lattice designs with micro-scale features were modelled and simulated using Fusion 360. A gyroid lattice pattern was chosen as this design supported drainage during the SLA printing process.

A disk measuring 23 mm in diameter and 1.5 mm in thickness was modelled as the base geometry. A volume lattice modifier was then applied to this geometry to create two gyroid lattice structures with lattice cell sizes of 1 mm and 0.5 mm, respectively. The gyroid track widths were set to 0.5 mm for the 1 mm cell size and 0.25 mm for the 0.5 mm cell size. All lattices were simulated with a fill factor of 0.5.

The volume lattice bodies were then converted into a high-resolution polygonal mesh, and a base plate was added beneath the lattices to improve adhesion to the build platform. The base plate had a diameter 25.4 mm and a thickness of 0.5 mm. Finally, both designs were exported as .STL files in preparation for printing. The lattice designs with the added base plate are shown in Fig. 2.

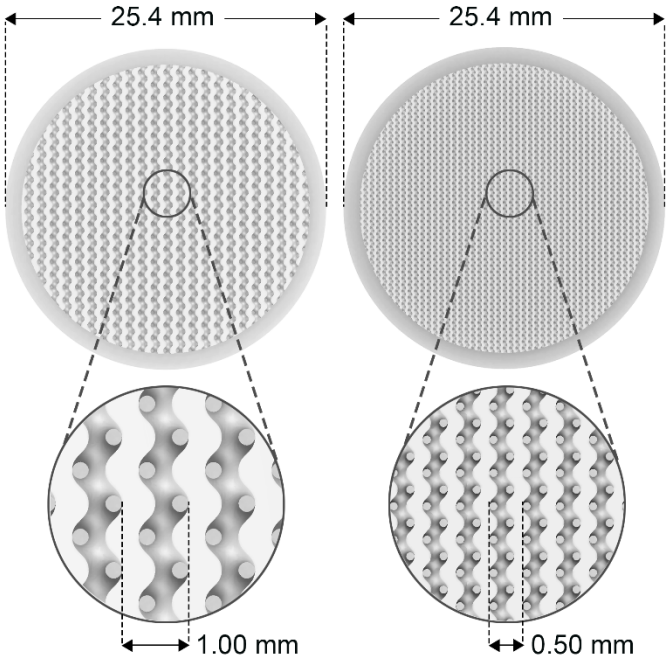

Fig. 2. Gyroid lattice designs with cell sizes of 1 mm (left) and 0.5 mm (right).

Optical Materials EXPRESS

2.3. Simulation of quasi-optical designs

To demonstrate how COR's optical properties can enable the production of cost-effective and complex quasi-optical components via SLA, a plano-convex lens and a Fresnel lens were developed based on the THz-TDS characterization results presented in Section 3.1 of this manuscript.

The plano-convex lens was designed using a simplified form of the lensmaker's equation, where (f) represents the focal length of the lens, (R) is the radius of curvature and (n) is the refractive index. The equation is given as:

$$R = (n - 1)f \tag{1}$$

The intended focal length of the plano-convex lens was 250 mm. As the operating frequency of the QCL system was 3.4 THz ($\lambda = 88$ microns), THz-TDS characterization determined COR to exhibit a refractive index of 1.562 at this frequency. Therefore, a radius of 140.5 mm was required to achieve the desired focal length.

Ansys Zemax OpticStudio (Version: 24 R1) was employed to simulate the CAD design for the Fresnel lens with a focal length of 50 mm. The refractive index of COR from 0.5–6.0 THz was added to the OpticStudio glass catalogue using the Fit Index data tool via the Schott dispersion formulae.

For the simulation, the beam aperture was set to 1.5 inches, and the operating wavelength was defined as 88 µm, aligning with the beam diameter and wavelength of the QCL system. The Fresnel 1 modifier was used to generate the lens design, with adjustments to the radius and number of zones to optimize performance.

The final design featured 15 Fresnel zones, with a defined radius of curvature of 28.5 mm. The thickness of the lens was 2 mm to ensure durability during thermal post-processing. When exporting the CAD file, the Fresnel zones were subdivided into 10 segments to enhance the resolution. A cross-section of the CAD design is shown in Fig. 3.

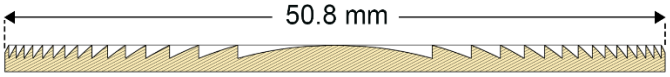

Fig. 3. Cross-section of the simulated Fresnel lens.

Both lenses were designed with a two-inch (50.8 mm) diameter to match commercially available lenses and ensure compatibility with existing lens mounts for the QCL system.

2.4. 3D printing process parameters

The chosen printer for this study was a Phrozen Sonic 4 K Mini Masked-Stereolithography (M-SLA) printer. To generate the slice files for the Sonic 4 K Mini, the build preparation software Chitubox was used (Version 1.8.1). The. STL files were imported into the software and oriented to optimize overall print time. The disks, lattices, and lenses were oriented horizontally to minimize the number of printing layers required. All designs were printed directly onto the build platform to enhance adhesion and to reduce the need for post-processing. No supporting structures were required for any of the designs.

To determine the exposure time required for the resin, the output power of the Sonic 4 K Mini was assessed using a PM100D power and energy meter (supplied by Thorlabs), equipped with an S120VC photodiode power sensor. The meter was calibrated to detect light at 405 nm, corresponding to the printer's output wavelength. To replicate standard printing conditions, the resin tray was installed, and the sensor was positioned above the build platform. Five measurements were taken, yielding an average reading of 0.9 mW. Owing to the sensor's circular

Optical Materials EXPRESS

aperture (9.5 mm diameter, 0.7088 cm^2 effective area), the UV power density was calculated as:

$$\frac{0.9\ mW}{0.7088\ cm^2} = 1.27\ mW/cm^2 \tag{2}$$

The supplier recommended an exposure dose of 250 mJ/cm^2 for adhesion layers and around 130 mJ/cm^2 for model layers. However, repeated print trials indicated that a base exposure time of 230 s (292.1 mJ/cm^2) and a layer exposure time of 120 s (152.4 mJ/cm^2) was optimal for achieving a 0.05 mm layer height. A base layer count of five was required to prevent delamination.

2.5. COR resin preparation and 3D printing

Prior to printing, the COR was removed from frozen storage. Appropriate Personal Protective Equipment (PPE) was worn at all times when working with the resin. This included nitrile gloves, safety glasses, a respirator and a laboratory coat, as recommended by the material's safety data sheet [34].

To thaw the resin, the aluminum cannister was placed into a preheated Carbolite Gero LHT oven, set to 40 °C for 1 hour. The cap of the cannister was loosened to prevent pressure buildup. Every 20 minutes the cannister was removed from the oven and shaken vigorously to ensure proper mixing of the resin. Fumes generated during the thawing process were vented into a fume cupboard.

To minimize exposure to resin vapors, the Sonic 4 K mini was setup in a fume cupboard to provide ventilation throughout the printing process. The build platform was levelled prior to installing the resin tank. A new Fluorinated Ethylene Propylene (FEP) film was fitted to the resin tank to ensure print quality. Finally, the tank was installed.

Once fully thawed the resin was poured into the printer's resin tank, it was then allowed to settle for 20 minutes, allowing air bubbles to dissipate before starting a print.

2.6. Post-processing stages

Following printing, the aluminium build platform was removed from the printer. Printed components remained attached to the build platform throughout all post-processing stages.

The printed parts were rinsed with a cleaning solvent, SupaRinse, supplied by polySpectra. Using a spray bottle, components were rinsed for around five minutes to remove any uncured resin. To ensure proper ventilation and to minimize exposure to fumes from the solvent and resin, this process was conducted in a fume cupboard.

To achieve the final thermomechanical properties of COR, a thermal post-cure is required. This is owing to the high glass transition temperature of the network, which would not be practical to achieve inside the printer itself. The build platform, with its polymer handle removed, was placed into a Heraeus Vacutherm VT 6060 vacuum oven, supplied by Thermo Fisher Scientific. The vacuum oven was preheated to 175 °C, and a vacuum was applied to reduce the pressure to below 5 mbar. Fumes emitted during the process were directed into a fume cupboard. The build platform remained in the oven under vacuum for 2 hours to complete the thermal post-cure. When complete the oven was switched off, and the platform and components were allowed to cool for 1 hour. The cooling process caused the aluminum plate to contract, allowing components to be removed with ease.

The printed lattice structures received no further post-processing. However, surface markings were visible on the base of the printed characterization disk and lenses, owing to direct printing onto the build platform. To ensure these surface defects did not impact the accuracy of optical measurements, the samples were polished to achieve a smoother surface.

A LaboSystem LaboPol-20 automatic polishing system, supplied by Struers, was used for surface finishing. The samples were initially polished using a 600-grit polishing wheel at 100 RPM for 2 minutes. This was followed by a final smoothing stage using a 1000-grit polishing

Optical Materials EXPRESS

wheel at 200 RPM for 2 minutes. A continuous water flow was applied throughout the processes to prevent overheating and to remove debris. The thickness of the characterization disk following polishing was 1.683 mm.

2.7. THz-TDS characterization of samples and THz-QCL characterization of quasi-optics

2.7.1. THz-TDS characterization

To determine the optical properties of COR at THz frequencies the printed disk was characterized using a THz-TDS system, which has been described in detail previously [35].

Initially a reference measurement was taken, with an empty optical path between the THz antenna and the detection system. For sample measurements the sample was mounted at the focus of the THz beam. To verify the optical properties, three measurements were performed on the printed samples, with each sample being moved in a vertical direction by 1 mm between each measurement. Spectral properties (absorption coefficient and refractive index) of the materials [36] are presented as an average of these three measurements in the frequency domain, with error bars shown as the standard deviation. The THz-TDS system was continuously purged with dry air to a relative humidity of <1% to remove water vapor absorption.

The THz-time-domain signal was collected over a measurement window of 110 ps, with a sampling step of 0.005 ps. To determine the complex permittivity of the sample, the time-domain data were Fast-Fourier transformed. A tukey window was applied, and data was zero-padded to provide a frequency resolution of 1 GHz. To estimate the noise level, the pre-pulse region of the signal was windowed and Fast-Fourier transformed; no further filtering or smoothing was applied. Across the measured frequency range, the THz beam diameter remained under 1 mm, significantly smaller than the diameter of the printed COR samples (25.4 mm).

All data is truncated to the frequency range over which measurements lie within the dynamic range of the system. This was determined by a comparison of the absorption spectrum with the maximal value as defined in [37].

2.7.2. THz-QCL lens power characterization

To evaluate the focusing capabilities of both COR lenses, the lenses were mounted in the beam-path of a QCL emitting at 3.4 THz (see Fig. 4). The QCL was housed inside a Janis ST-100 helium cryostat, and the temperature was maintained at 33 K throughout all measurements. Full specifications of the 3.4 THz QCL are reported in [38].

It was driven electronically with a 167 Hz, 700 mA square wave using a Wavelength Electronics QCL1000 LAB current source.

The THz beam emitted from the QCL was first collected and collimated using a 1.5-inch-diameter off-axis gold-coated parabolic mirror. After collimation, the beam was focused onto a pyroelectric detector using the printed lens under test. The detector was mounted on a motorized linear translation stage, allowing precise movement along the optical (z) axis, the direction of THz beam propagation, to accurately position the detector at the beam focus. The setup with the installed COR Fresnel lens is shown in Fig. 5.

Signal demodulation was performed using a Signal Recovery 7265 lock-in amplifier, referenced to the 167 Hz modulation frequency provided by the signal generator. The lock-in amplifier was configured with a sensitivity of 50 mV and a time constant of 200 ms, and the demodulated output voltage was recorded in millivolts (mV).

To study the beam focusing behavior, the detector was systematically moved along the z-axis, and the signal amplitude was recorded as the detector passed through the focal point. Baseline measurements were first recorded without the lenses installed to establish a reference for comparison.

Optical Materials EXPRESS

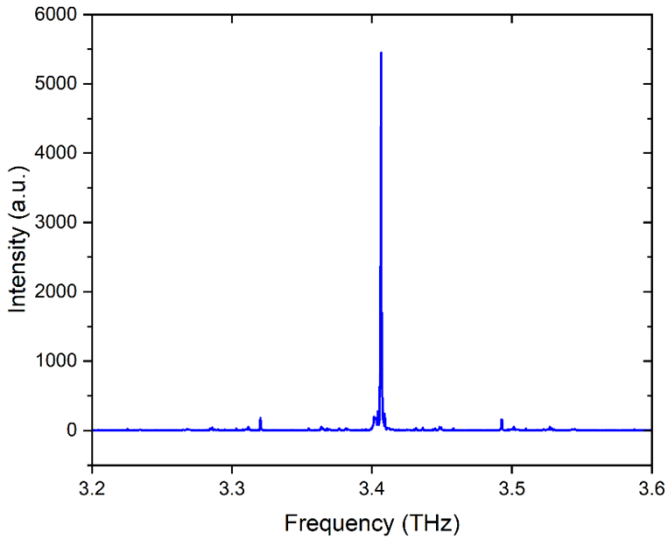

Fig. 4. Emission spectra of the QCL at 3.4 THz, operating at 33 K and a bias current of 700 mA.

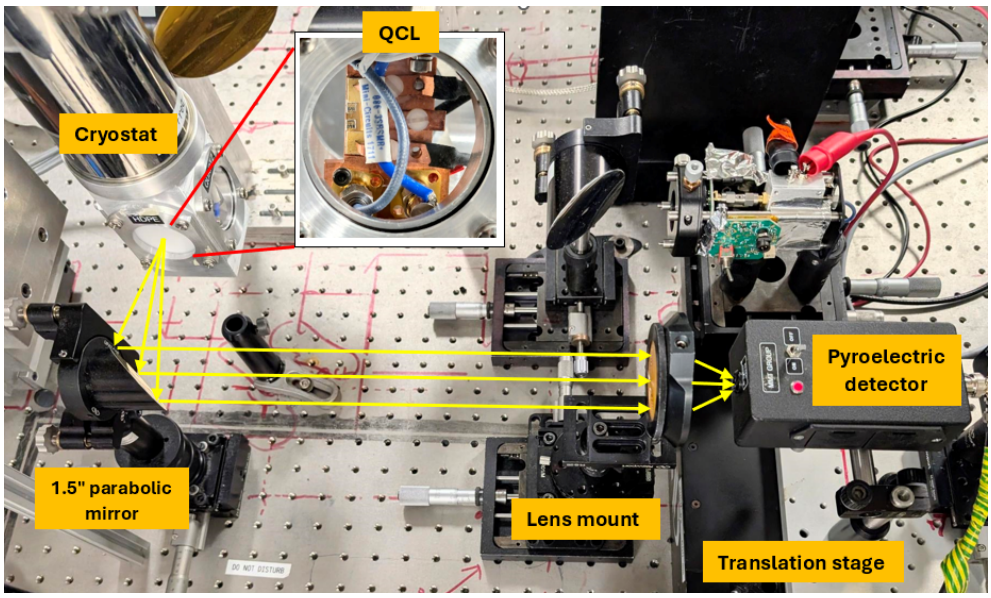

Fig. 5. Experimental setup showing the optical lens system used to direct the 3.4 THz beam emitted from the QCL.

Optical Materials EXPRESS

The signal power (P_{THz}) in milliwatts (mW) was determined from the demodulated detector voltage (V_{d}) in mV and the responsivity of the detector $R_{\mathrm{V}} = 6.04$ V/W:

$$P = V_d/R_V \tag{3}$$

2.7.3. THz QCL beam profiling

For beam profile characterization of the COR Fresnel lens, the lens was mounted in a separate QCL system with a slightly modified configuration compared to the setup used for the power measurements (see Fig. 6). The Plano-convex lens was not included in these measurements, as its focal length exceeded the maximum travel range of the translation stage.

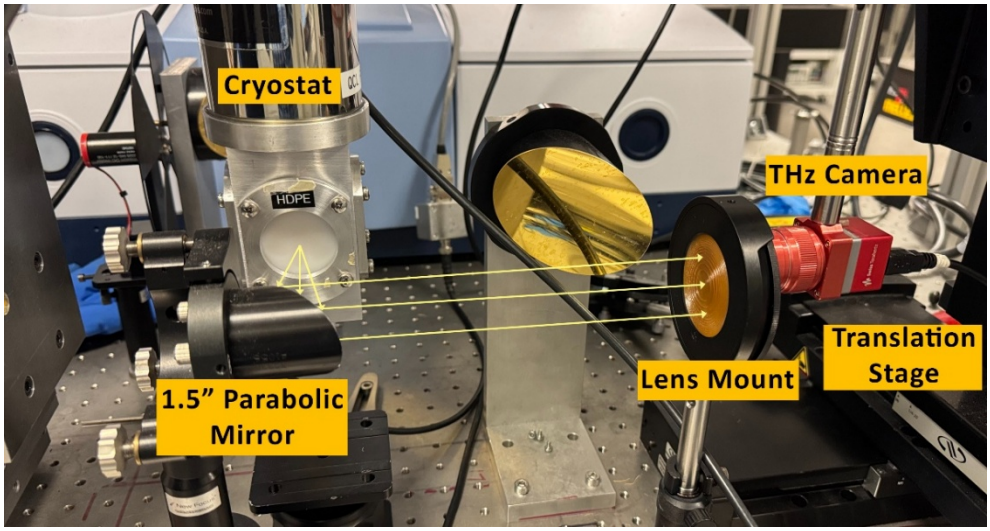

Fig. 6. Experimental setup illustrating the layout used to guide the 3.52 THz beam emitted by the QCL through the COR Fresnel lens to the THz camera.

The radiation source in this system was a 3.52 THz QCL operating in continuous wave mode, housed within a cryogenic system maintained at 20 K throughout all measurements. The full specifications of the 3.52 THz QCL are reported in [39]. The QCL was driven by an Arroyo Instruments 4302 current source at a bias current of 900 mA and a voltage of 9.056 V.

A THz camera (Rigid S2, Swiss Terahertz) was used to capture two-dimensional images and evaluate the transmitted beam after passing through the lens at various focal distances, providing spatial information on the beam shape and intensity distribution.

Images were captured at axial distances between 45 mm and 80 mm from the lens position to measure the propagation of the beam around the expected ~50 mm focal length. Measurements were taken in 5 mm increments between 45 mm and 55 mm to identify the beam waist position, and in 10 mm increments between 60 mm and 80 mm to determine the divergence angle. At each position, the full width at half maximum (FWHM) beam diameters along the X and Y axes were recorded.

2.8. Optical characterization of 3D printed lattice structures

To examine the micro features of the printed lattice structures, an Olympus BX53M upright optical microscope was used, equipped with a SC50 5-megapixel camera for capturing digital images. The lattices were inspected at 2.5 × magnification.

The Olympus Stream Essentials software was used to analyze and record images of the samples. Multiple images were taken at varying focal planes and combined into a composite image using

Optical Materials EXPRESS

the extended focal imaging module. The resulting measurements were compared against the dimensions of the CAD models to validate the accuracy of scale bars.

Dimensional measurements were recorded from the optical microscope images using the ImageJ software package. The scale bar from captured images was used to calibrate the software for accurate measurements.

3. Results

3.1. THz-TDS characterization results

Figure 7 presents the Fourier-transformed THz-TDS results, showing the mean absorption coefficients and refractive indices of the COR sample from 0.5 to 6.0 THz, averaged from three measurements.

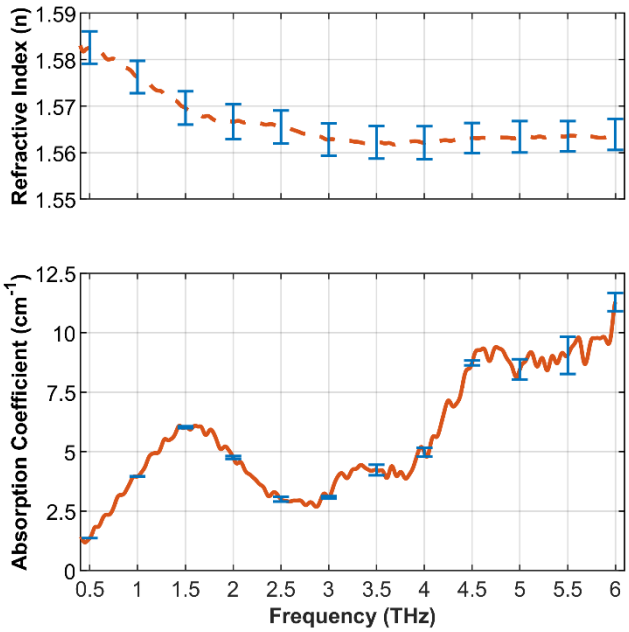

Fig. 7. THz time-domain spectroscopy results. Mean refractive indices (dashed lines, upper subplot) and absorption coefficients (solid lines, lower subplot) of COR samples from 0.5 to 6.0 THz. Error bars represent the standard deviation from three measurements.

At 1 THz the sample exhibited an absorption coefficient of $(3.96 \pm 0.01)\ \mathrm{cm}^{-1}$, considerably lower than AM photopolymers which typically have an absorption coefficient exceeding $19\ \mathrm{cm}^{-1}$ at the same frequency [17]. From 1.5 to 3.0 THz the absorption coefficient decreased from $(6.03 \pm 0.04)\ \mathrm{cm}^{-1}$ to $(3.08 \pm 0.06)\ \mathrm{cm}^{-1}$. At 6.0 THz the absorption coefficient rose to $(11.3 \pm 0.4)\ \mathrm{cm}^{-1}$. For comparison, standard photopolymers have been shown to have absorption coefficients greater than $100\ \mathrm{cm}^{-1}$ at 4 THz [19].

The sample's refractive index steadily decreased from 0.5–6.0 THz, from 1.583 ± 0.004 to 1.564 ± 0.003. The most notable change was from 0.5–2.0 THz (1% change), with the refractive index being relatively stable from 2.0–6.0 THz (0.18% change). Duangrit et al. found standard AM photopolymers exhibit refractive indices between 1.61 and 1.72 at 1 THz [18].

Optical Materials EXPRESS

3.2. Printed COR lattices

The printed lattice structures following post-processing are shown in Fig. 8. Both the 1 mm and 0.5 mm cell size lattice designs printed successfully and withstood thermal post-processing. The gyroid pattern is clearly visible in both samples.

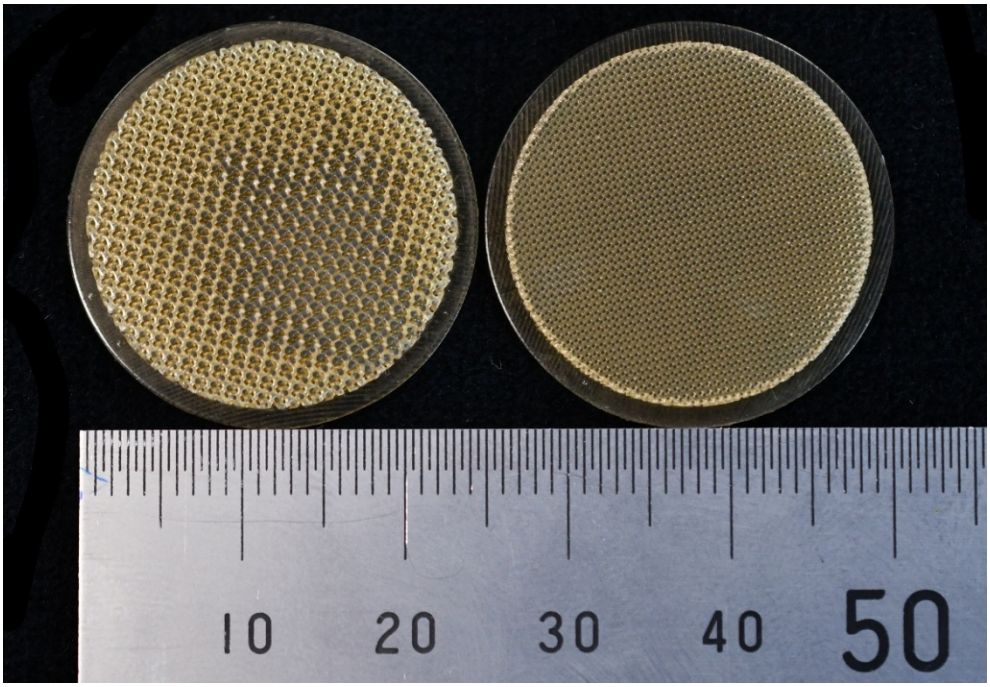

Fig. 8. Printed COR lattice designs following post-processing: 1 mm cell size (left) and 0.5 mm cell size (right). A scale indicator is included with measurements in millimeters.

Figure 9 presents the captured optical microscope images of both lattice designs at 2.5× magnification. Figure 9(A) shows the 1 mm cell size lattice, while Fig. 9(B) showcases the 0.5 mm cell size lattice. Four measurements of the lattice track widths were recorded for each image using Image J.

The 1 mm cell size lattice was intended to have track widths of 500 µm, while analysis showed a mean value of 508.1 µm (1.62% percentage error). The 0.5 mm cell size lattice was intended to have a track width of 250 µm, with image analysis showing a mean value of 266.3 µm (6.52% percentage error). Despite these slight deviations, the micro-features of both lattices were well-formed and demonstrated repeatability.

3.3. Performance characterization of 3D-printed COR quasi-optical components

The printed COR plano-convex and Fresnel lenses are presented in Fig. 10. As shown, both lenses successfully printed. No thermal defects were observed following the thermal post-processing stage.

Figure 11 presents the results from the QCL characterization at 3.4 THz, as measured using the pyroelectric detector, with signal power (mW) plotted for various system configurations.

Panel A presents a baseline scan of the system with no lens in the beam path, with the detector positioned along the z-axis from 150 mm to 300 mm. As expected, the signal power decreases with distance, falling from 3.43 mW at 150 mm to 0.25 mW at 300 mm.

Optical Materials EXPRESS

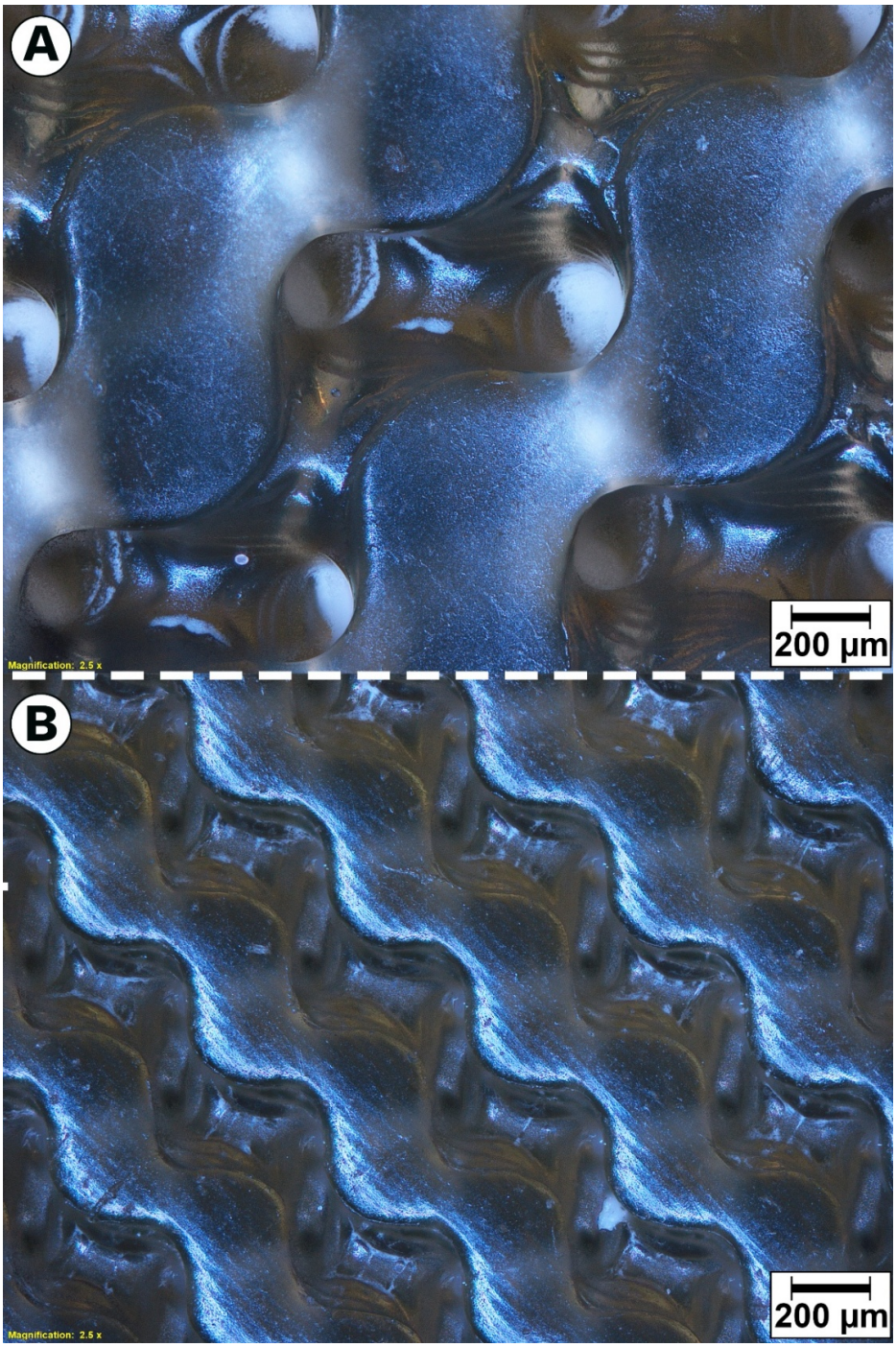

Fig. 9. Optical microscopy images at 2.5 × magnification of printed COR lattices. (A) 1 mm lattice cell size. (B) 0.5 mm lattice cell size.

Optical Materials EXPRESS

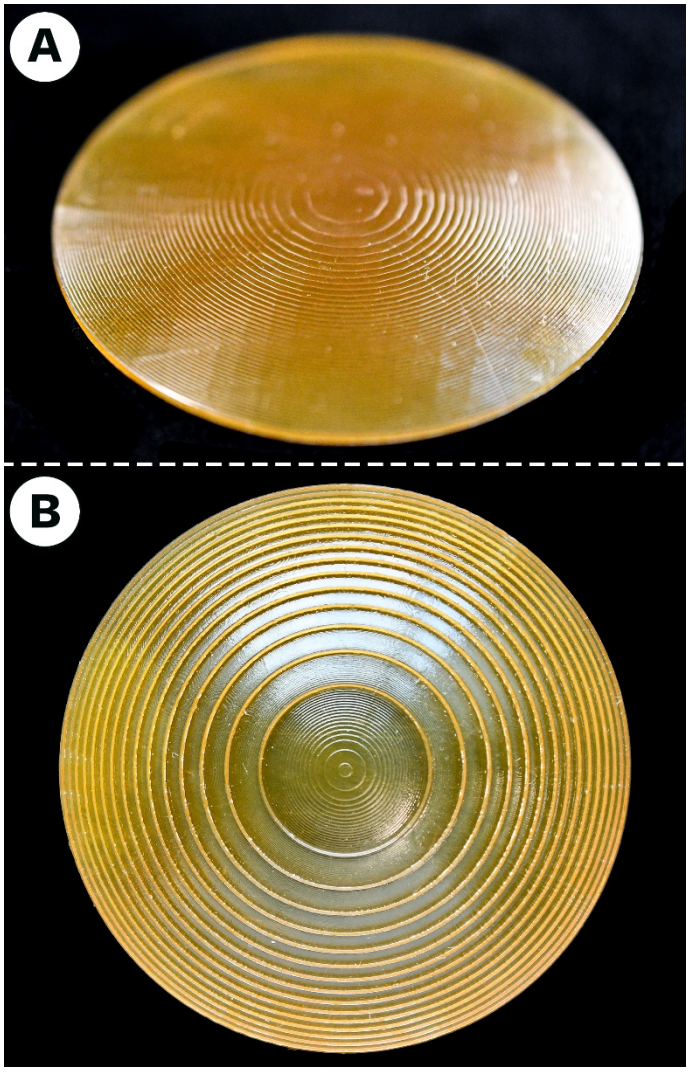

Fig. 10. Photographs of the 3D-printed COR lenses. Panel A presents the plano-convex lens, while panel B shows the Fresnel lens.

Panel B presents the corresponding measurements with the COR plano-convex lens installed, with the same detector positions as in Panel A. A peak signal of 3.70 mW is observed at 210 mm.

Panel C depicts a second baseline scan of the system without a lens over a shorter z-axis range from 35 mm to 70 mm. The signal power decreases from 12.59 mW at 35 mm to 9.52 mW at 70 mm.

Panel D shows the corresponding measurements with the COR Fresnel lens mounted. The Fresnel lens demonstrated high efficiency, with the signal power increasing significantly to a peak of 39.54 mW at 50 mm.

Figure 12 presents the gain profiles of each lens, calculated by normalizing the measured signal power against the respective baseline scans. A Gaussian fit was added to highlight the focusing behavior of each lens.

Panel A shows the plano-convex lens gain, with a distinct peak of 6.90 observed at an axial distance of 240 mm. The signal gain remains above 6.0 between 230 mm to 260 mm. Panel B

Optical Materials EXPRESS

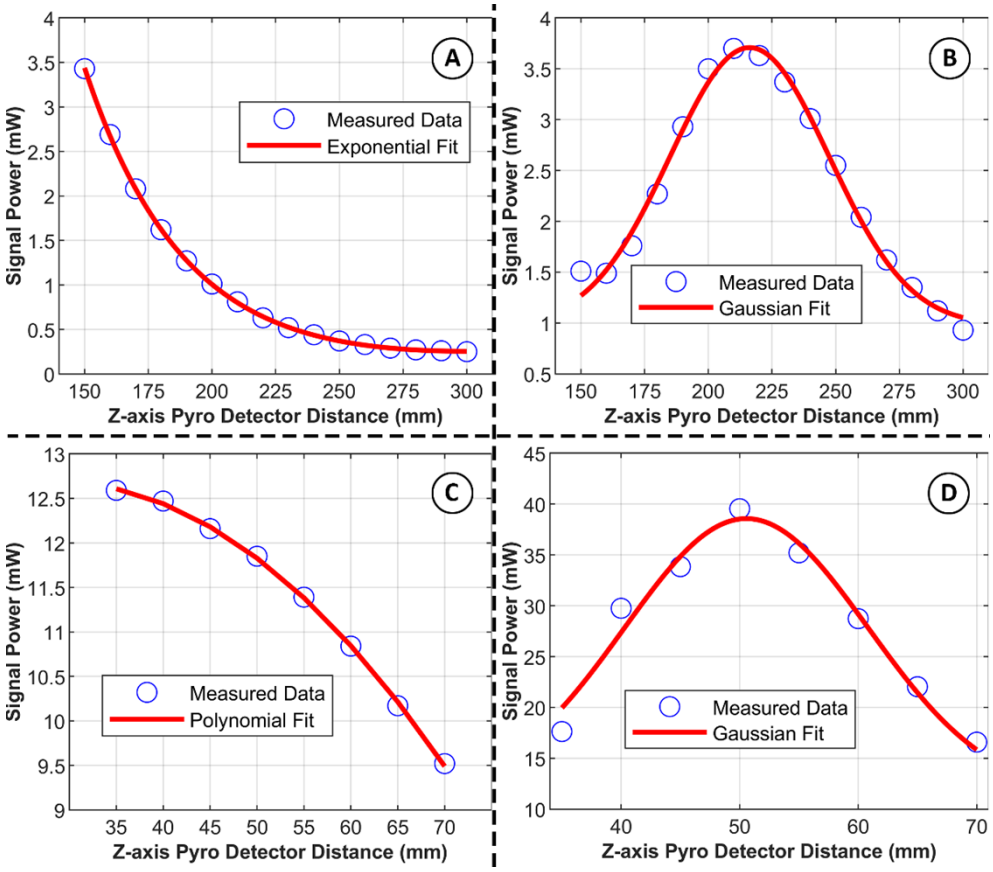

Fig. 11. Signal power measurements from QCL testing at 3.4 THz using a pyroelectric detector. Panels A and C show reference scans of the QCL system without lenses installed. Panel A is fitted using a two-term exponential fit, while Panel C is fitted with a second-order polynomial fit (poly2). Panel B shows the results with the COR plano-convex lens installed, fitted using a four-parameter Gaussian model with offset ($a = 2.73$, $b = 216.2$, $c = 44.18$, $d = 0.98$). Panel D shows the results with the Fresnel lens installed, also fitted using a four-parameter Gaussian model with offset ($a = 27.27$, $b = 50.56$, $c = 14.53$, $d = 11.29$).

presents the Fresnel lens gain, with a peak value of 3.34 at a z-axis distance of 50 mm. A signal gain above 3.0 was observed between a distance of 50 mm and 55 mm.

These gain profiles confirm that both lenses function as designed, with peak focusing observed close to their respective intended focal distances, 250 mm for the plano-convex lens and 50 mm for the Fresnel Lens.

3.4. THz QCL beam profile with a 3D-printed COR Fresnel lens

The THz QCL (3.52 THz) beam profile images captured by the THz camera at different z- axis positions after passing through the Fresnel lens are shown in Fig. 13. A 3D visualization of the beam profile is shown in Fig. 14. The Fresnel lens effectively reduced the THz beam diameter from an initial width of approximately 38.1 mm to a focused beam with a diameter of less than 3 mm, between axial positions of 50 mm and 80 mm. Diffraction patterns, including ring-like structures are visible in all images, these are expected owing to the diffractive nature of Fresnel lenses.

Optical Materials EXPRESS

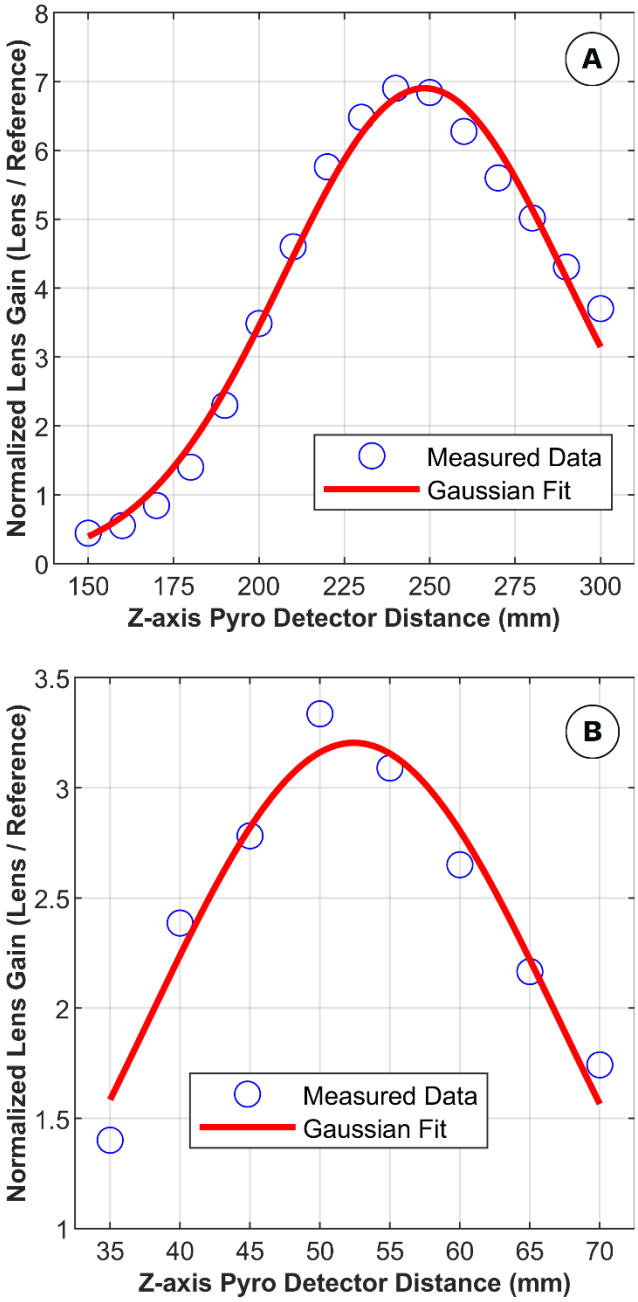

Fig. 12. Signal gain of each lens normalized against the reference scan from QCL testing at 3.4 THz using a pyroelectric detector. Panel A shows the gain profile for the plano-convex lens, fitted using a three-parameter Gaussian model without an offset (a = 6.902, b = 248.4, c = 58.16). Panel B shows the gain profile for the Fresnel lens, also fitted using a three-parameter Gaussian model without an offset (a = 3.204, b = 52.42, c = 20.76).

Optical Materials EXPRESS

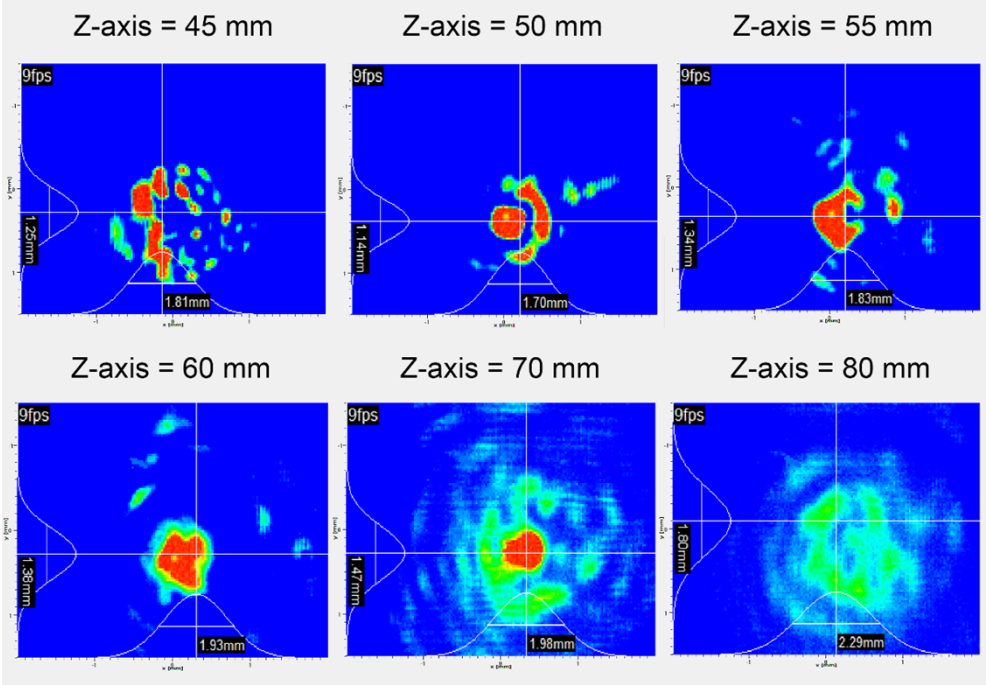

Fig. 13. COR Fresnel lens beam profile images captured using the THz camera during QCL characterisation at 3.52 THz.

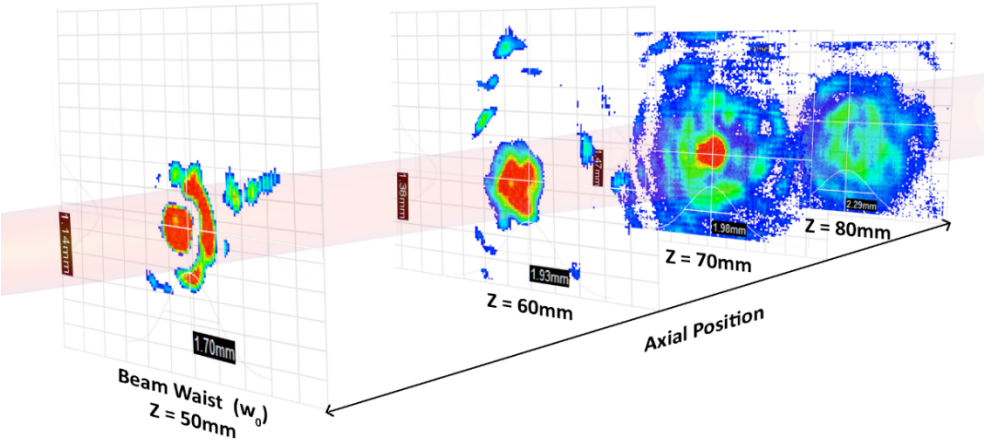

Fig. 14. 3D Visualization of the COR Fresnel lens beam profile images captured with the THz camera during QCL characterization at 3.52 THz.

Optical Materials EXPRESS

The FWHM beam diameter measurements obtained from the THz camera were converted to the corresponding $1/e^2$ beam radii. Owing to differences in diameter along the X and Y axes, both values were converted separately. The recorded values were then scaled by a factor of 0.8493, assuming a Gaussian beam profile, to determine the $1/e^2$ beam radius. The resulting values are presented in Table 1.

Table 1. Measured FWHM beam diameters (X and Y) and corresponding $1/e^2$ beam radii of the 3.52 THz QCL beam after transmission through the Fresnel lens, recorded at various axial positions

Focal Distance (mm)	X-axis FWHM Beam Diameter (mm)	Y-axis FWHM Beam Diameter (mm)	X-axis Corresponding $1/e^2$ Beam Radii (mm)	Y-axis Corresponding $1/e^2$ Beam Radii (mm)
45	1.81	1.25	1.54	1.06
50	1.70	1.14	1.44	0.97
55	1.83	1.34	1.55	1.14
60	1.93	1.38	1.64	1.17
70	1.98	1.47	1.68	1.25
80	2.29	1.80	1.94	1.53

The corresponding beam profiles, derived from the THz camera images, are shown in Fig. 15. Panel A presents the $1/e^2$ beam radius along the X-axis, while panel B shows the $1/e^2$ beam radius along the Y-axis. Although slight astigmatism was observed in the beam profile, the minimum beam waist was identified at a Z-axis position of 50 mm, with beam waist values of 1.44 mm and 0.97 mm for the X and Y axes, respectively.

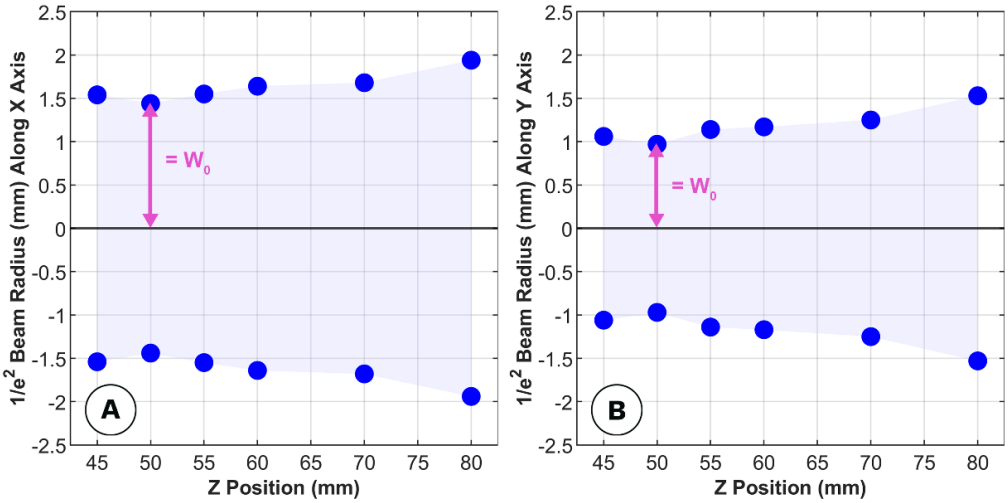

Fig. 15. Beam profile of the COR Fresnel lens showing the $1/e^2$ beam radii at axial positions from 45 mm to 80 mm. Panel A shows the beam radius along the X axis; Panel B shows the beam radius along the Y axis.

The beam waist was observed at the intended focal length of the printed Fresnel lens, confirming the lens successfully focused the 3.52 THz QCL beam as designed. However, scattering or diffraction from the Fresnel lens ridges may have influenced the measured beam radius. Additionally, the observed astigmatism could be attributed to the quality of the incident beam emitted by the QCL.

Optical Materials EXPRESS

4. Discussion

4.1. THz-TDS characterization results

The THz-TDS characterization results demonstrate that COR exhibits an absorption coefficient of approximately 4 cm^{-1} at 1 THz and 11 cm^{-1} at 6 THz. As shown in Fig. 16, this represents a significant decrease when compared to standard AM photopolymers at 1 THz. Additionally, the absorption coefficient of COR at 1 THz is comparable to that of PTFE (2.6 cm^{-1}) and silica (2.94 cm^{-1}), both of which are conventionally molded into THz optics and widely used in THz systems.

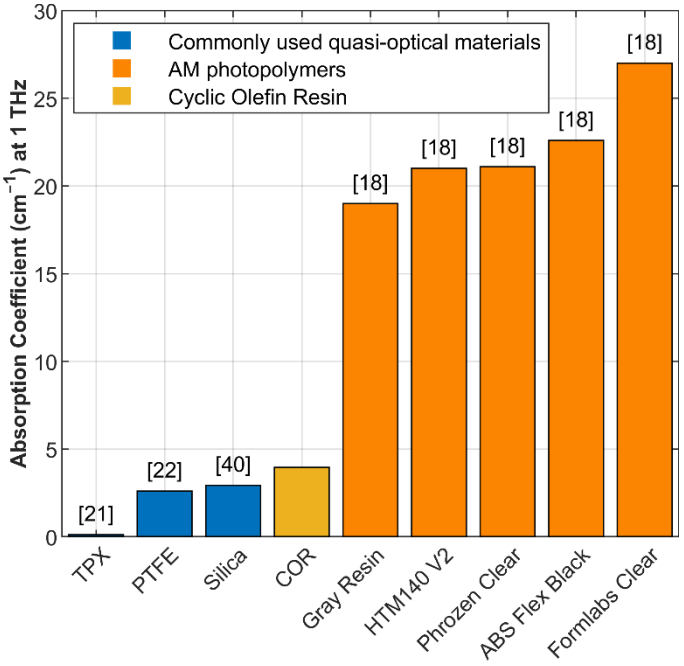

Fig. 16. Comparison of the absorption coefficients at 1 THz of conventionally used quasi-optical materials, AM photopolymers, and the Cyclic Olefin Resin characterized in this study. Values for quasi-optical materials and AM photopolymers were obtained from references cited in [18,21,22,40]

The absorption coefficient of standard AM photopolymers at 2 THz has been reported to range between 60 cm^{-1} and 68 cm^{-1} [19,20], whereas COR exhibits a significantly lower value of around 4 cm^{-1}. Few studies have successfully characterized AM photopolymers beyond 2 THz, due to their low transparency and the need for extremely thin samples to compensate for high absorption.

The transmittance values of COR and photopolymers from the literature were calculated using Eq. (4), based on the Beer-Lambert Law, with α representing the absorption coefficient and d the sample thickness. Based on these results, a COR sample with a 1 mm thickness would exhibit a transmission of 67.31% at 1 THz, decreasing to 62.16% at 2 THz. For comparison standard AM photopolymers would exhibit transmittance values ranging from 6.72% to 14.96% at 1 THz, decreasing to between 0.25% and 0.11% at 2 THz.

$$T = e^{-\alpha d} \tag{4}$$

The enhanced transmission of COR is advantageous for the AM and THz communities, positioning COR as a highly desirable material choice for quasi-optical applications. This

Optical Materials EXPRESS

advancement enables the production of SLA-produced optics with significantly improved performance, reducing quasi-optical loss in THz systems. The reduced absorption between 2 and 5 THz also makes COR optics highly suitable for THz QCL systems, which typically operate within this frequency range [41].

The refractive index of COR was shown to be stable from 0.5–6.0 THz, decreasing slightly from 1.583 to 1.564. This minimal change suggests low dispersion, demonstrating the material to be well-suited for broadband THz optical applications. Lenses produced from COR would require minimal adjustments across this bandwidth.

However, COR exhibited a refractive index around 1.58 at 1 THz, whereas standard photopolymers range from 1.61 to 1.72 at the same frequency [17]. Therefore, COR lenses would need to be slightly thicker than standard photopolymer lenses to achieve a comparable focal length. However, this increase in thickness would have a negligible effect on transmission.

4.2. Optical characterization of COR lattices

Optical characterization of the printed COR lattices demonstrated that geometric features with feature sizes below the wavelength scale of 1 THz ($\lambda = \sim 300\,\mu m$) can be successfully and repeatably manufactured via stereolithography and survive the thermal post-processing stage. Both lattices with micro-features showed minimal variation in scale. This high resolution could be leveraged to allow for the fabrication of more complex quasi-optical designs, including Gradient-Index (GRIN) and Fresnel axicon lenses to be produced via low-cost SLA systems. However, the M-SLA system used in this study was limited to an XY resolution of 35 µm, which constrained the minimum achievable feature size.

4.3. Evaluation of COR quasi-optics

The QCL characterization results demonstrated that both COR lenses effectively focused THz radiation, achieving maximum signal gain close to their intended focal lengths, when normalized against the reference scan.

The plano-convex lens exhibited a peak signal gain of 6.90 at a focal distance of 240 mm, closely matching the intended focal length of 250 mm. The slight deviation may be attributed to the lens's thin profile and large radius of curvature, which require tight manufacturing tolerances. Although no thermal defects were observed, minor variations in curvature or dimensional accuracy during printing or post-processing may have contributed to this.

The Fresnel lens closely matched its design parameters, achieving a peak signal gain of 3.34 at a focal length of 50 mm. Beam profile images confirmed that it effectively reduced an approximately 1.5-inch diameter incident beam to a beam waist of less than 2 mm at the focal point of the lens. As expected, diffractive effects were observed in the beam profile images due to the diffractive behavior of Fresnel lenses. The successful fabrication of a functional Fresnel lens highlights AM's capability to produce bespoke optical components at low-cost.

These results demonstrate that the high transparency of COR at THz frequencies can be leveraged to manufacture efficient and complex quasi-optical components using consumer-grade SLA printers. Production of bespoke quasi-optical designs on SLA systems could be readily scaled, potentially lowering costs and increasing the accessibility and diversity of available THz quasi-optical components. Additionally, compact SLA systems could facilitate localized production of optics, further enhancing accessibility.

4.4. Material considerations and perspectives for future study

A drawback of processing COR via SLA is the high exposure dose required to initiate polymerization per 0.05 mm layer (152.4 mJ/cm^2), which significantly reduces throughput. For comparison, commercially available AM resins typically require an exposure dose of less than 20 mJ/cm^2 for cure depths around 200 microns, leading to significantly faster print times [42]. However,

Optical Materials EXPRESS

the extended exposure time is influenced by the optical power density of the Sonic Mini 4 K (1.27 mW/cm^2). A system with a more powerful 405 nm UV source could drastically reduce the exposure time per layer, thereby improving throughput. An advantage of processing COR via a M-SLA system is its ability to print multiple components simultaneously within the same build time. For batch production, this capability could be leveraged to increase throughput.

Another limitation of COR is the need for a thermal post-processing treatment in a vacuum oven. Samples manufactured in this study were printed directly to the build plate and underwent thermal treatment while still attached, reducing the risk of thermal defects. Vertically orientated components with thin-walled features may be prone to warping, limiting the scope of printable optical designs. However, polySpectra the supplier of the resin does offer a solution that allows the thermal post-processing cycle to be performed in a standard microwave or oven while submerged in their proprietary solution (waveCure). This alternative may reduce thermal defects, but future research is required to determine if changes to the post-processing stages impact the optical properties of COR at THz frequencies.

The COR Alpha photopolymer characterized in this study is a translucent yellow in its printed state, unlike many bulk COC polymers which are visually transparent. Variations of COR are also available from the supplier in a range of colors. However, characterization of these COR formulations would be required to determine if changes in their formulation impact SLA processing or the THz properties of printed samples.

Despite the low throughput and the added post-processing stages, the optical properties of COR represent an advantage for the AM and THz communities. COR's transparency is significantly higher than commercially available photopolymer resins in the THz region and is a more viable solution than ceramic-filled photopolymers, which introduce scattering effects during printing and reduce geometric accuracy due to refractive index mismatches between photopolymers and ceramics at 405 nm. COR could, therefore, enable the production of efficient, low-loss quasi-optical components with smooth surfaces and intricate features using low-cost SLA systems.

Future work could explore the potential of filler materials to tailor the optical properties of COR. Due to its high transparency, the resin could effectively serve as a transparent binder. Incorporating high refractive index fillers could enable the development of COR composites with higher refractive indices at THz frequencies, which may be beneficial for a variety of quasi-optical applications.

5. Conclusion

This study investigated the THz properties of a COR compatible with SLA 3D printers, evaluating its potential to produce THz quasi-optical components.

Through the fabrication of samples via a M-SLA system and THz characterization using a THz-TDS system, COR was shown to exhibit exceptional transparency to THz radiation from 0.5–6 THz, with absorption coefficients of approximately 4 cm^{-1} at 1 THz and ~ 11 cm^{-1} at 6 THz. Additionally, printed COR lattices were optically inspected, showing consistent and repeatable features with sizes below 300 µm.

The fabrication and evaluation of custom plano-convex and Fresnel lenses demonstrated that SLA-processed COR optics can be used to produce functional, efficient, and geometrically complex quasi-optical designs operational at 3.4 THz. The plano-convex lens achieved a peak signal gain of 6.90 at 240 mm, while the Fresnel lens reached 3.34 at 50 mm, both closely matching their intended focal lengths, confirming their performance.

These findings represent a significant breakthrough, as COR was shown to be considerably more transparent to THz radiation than standard photopolymers with an absorption coefficient comparable to that of non-polar polymers at THz frequencies. Evaluation of the lenses

Optical Materials EXPRESS

demonstrated how COR can be processed to produce bespoke, complex and efficient quasi-optical components via-low-cost SLA systems, enabling localized manufacturing of THz optics.

However, the exposure required to initiate cross-linking of COR was significantly higher than that of standard photopolymers, reducing throughput considerably. The requirement for a thermal bake of printed components could also introduce thermal defects to select quasi-optical designs.

Future work could identify methods to increase printing speeds to ensure scalability. New ways to leverage the transparency of COR could also be explored, including the development of COR composites with tailored optical properties.

Funding. UK Research and Innovation (MR/S016969/1, MR/Y011775/1).

Acknowledgements. The authors gratefully acknowledge financial support from UK Research and Innovation (Future Leader Fellowship MR/S016969/1 and MR/Y011775/1) and a Doctoral Scholarship from The School of Mechanical Engineering, University of Leeds, U.K. We sincerely thank Lee Wetherill, the laboratory manager, for his invaluable support throughout the experimental work. We also extend our gratitude to Rhys Moore and James Watkins for their advice and assistance with additive manufacturing. Special thanks to Jay Ward for his technical expertise and help with post-processing the material. Additionally, we thank Brian Leal from polySpectra for his technical support. **Permission to reproduce material from other sources**. Some material has been reproduced under the Creative Commons Attribution-NonCommercial-NoDerivatives 4.0 International Licence (CC-BY-NC-ND 4.0) from American Chemical Society (Fig. 1). Full citations for the original images are given in the respective captions.

Disclosures. The author Raymond A. Weitekamp has an ownership interest in polySpectra, which develops the materials tested in this study. However, all testing and analysis were conducted independently. No financial support was received from polySpectra for this work.

The authors declare no other conflicts of interest.

Data availability. The data associated with this paper is openly available in the University of Leeds data repository [43].

References

1. J. Wang, M. Naftaly, and E. Wasige, "An Overview of Terahertz Imaging with Resonant Tunneling Diodes," Appl. Sci. **12**(8), 3822 (2022).
2. M. Jazbinsek, U. Puc, A. Abina, *et al.*, "Organic Crystals for THz Photonics," Appl. Sci. **9**(5), 882 (2019).
3. A. J. Fitzgerald, E. Berry, N. N. Zinovev, *et al.*, "An introduction to medical imaging with coherent terahertz frequency radiation," Phys. Med. Biol. **47**(7), R67–R84 (2002).
4. X. Li, J. Li, Y. Li, *et al.*, "High-throughput terahertz imaging: progress and challenges," Light: Sci. Appl. **12**(1), 233 (2023).
5. C. K. Kundu, W. He, R. Yu, *et al.*, "Terahertz Waves and Their Applications in Textiles and Composites: Advances and Practical Insights," Adv. Mater. Technol. **10**(23), 2400738 (2025).
6. B. Zhang, W. Chen, Y. Wu, *et al.*, "Review of 3D Printed Millimeter-Wave and Terahertz Passive Devices," Int. J. Antennas Propag **2017**, 1–10 (2017).
7. B. Scherger, S. Wietzke, M. Scheller, *et al.*, "Characterization of Micro-Powders for the Fabrication of Compression Molded THz Lenses," J. Infrared Millim. Terahertz Waves **32**(7), 943–951 (2011).
8. B. Scherger, M. Scheller, C. Jansen, *et al.*, "Terahertz lenses made by compression molding of micropowders," Appl. Opt. **50**(15), 2256–2262 (2011).
9. Q. Xu, Y. Lu, X. Feng, *et al.*, "Recent Advances on Terahertz Wave Generation and Synchronous Control," Adv. Opt. Mater. **14**(10), 2501920 (2026).
10. J. A. Byford, Z. Purtill, and P. Chahal, "Fabrication of Terahertz Components Using 3D Printed Templates," in *Proceedings - Electronic Components and Technology Conference*, 817–822 (2016).
11. J. Sun and F. Hu, "Three-dimensional printing technologies for terahertz applications: A review," Int. J. RF Microw. Comput.-Aided Eng **30**(1), e21983 (2020).
12. M. Kaluza, M. Walczakowski, and A. Siemion, "Exploring the Impact of 3D Printing Parameters on the THz Optical Characteristics of COC Material," Materials **17**(20), 5104 (2024).
13. S. M. Latifi, P. Torkaman, E. García-Tuñón, *et al.*, "Refractive Index Engineering of 3D-Printing Terahertz Composite Materials," Adv. Mater. Technol. **10**(14), 2500344 (2025).
14. A. D. Squires, E. Constable, and R. A. Lewis, "3D Printed Terahertz Diffraction Gratings And Lenses," J. Infrared Millim. Terahertz Waves **36**(1), 72–80 (2015).
15. A. Kaur, J. C. Myers, M. I. M. Ghazali, *et al.*, "Affordable terahertz components using 3D printing," in *Proceedings - Electronic Components and Technology Conference*, 2071–2076 (2015).
16. A. Shrotri, B. Krause, O. Stübbe, *et al.*, "Evaluation of Additively Manufactured Axicon Lenses Using a THz-Camera," in *49th International Conference on Infrared, Millimeter, and Terahertz Waves (IRMMW-THz)* (2024).
17. L. Phillips, A. Valavanis, A. D. Burnett, *et al.*, "Process and material constraints of additive manufacturing for fabrication of terahertz quasi-optical components," Appl. Mater. Today **42**, 102619 (2025).

Optical Materials EXPRESS

18. N. Duangrit, B. Hong, A. D. Burnett, *et al.*, "Terahertz Dielectric Property Characterization of Photopolymers for Additive Manufacturing," IEEE Access **7**, 12339–12347 (2019).
19. L. Phillips, A. Valavanis, A. D. Burnett, *et al.*, "Innovative Approaches to Fabricate Terahertz Optics with Additive Manufacturing: Manufacture and THz Characterisation of a Silica-Filled Photopolymer," in *Proceedings of the 35th Annual International Solid Freeform Fabrication Symposium* (University of Texas at Austin, 2024), pp. 629–636.
20. C. H. Brodie, I. Spotts, H. Reguigui, *et al.*, "Comprehensive study of 3D printing materials over the terahertz regime: absorption coefficient and refractive index characterizations," Opt. Mater. Express **12**(9), 3379 (2022).
21. M. Naftaly, R. E. Miles, and P. J. Greenslade, "THz transmission in polymer materials — a data library," in *Joint 32nd International Conference on Infrared and Millimeter Waves*, 819–820 (2007).
22. P. D. Cunningham, N. N. Valdes, F. A. Vallejo, *et al.*, "Broadband terahertz characterization of the refractive index and absorption of some important polymeric and organic electro-optic materials," J. Appl. Phys. **109**(4), 043505 (2011).
23. A. Podzorov and G. Gallot, "Low-loss polymers for terahertz applications," Appl. Opt. **47**(18), 3254–3257 (2008).
24. J. Bichon, A. Pillet, A. Sklia, *et al.*, "Complex refractive index determination of PTFE, TPX and polypropylene windows for TeraHertz broadband spectroscopy," in *47th International Conference on Infrared, Millimeter, and Terahertz Waves (IRMMW-THz)* (2022).
25. G. Pastorelli, T. Trafela, P. F. Taday, *et al.*, "Characterisation of historic plastics using terahertz timedomain spectroscopy and pulsed imaging," Anal. Bioanal. Chem. **403**(5), 1405–1414 (2012).
26. S. F. Busch, M. Weidenbach, J. C. Balzer, *et al.*, "THz Optics 3D Printed with TOPAS," J. Infrared Millim. Terahertz Waves **37**(4), 303–307 (2016).
27. E. Mavrona, J. Graf, E. Hack, *et al.*, "Optimized 3D printing of THz waveguides with cyclic olefin copolymer," Opt. Mater. Express **11**(8), 2495 (2021).
28. R. A. Weitekamp, H. A. Atwater, and R. H. Grubbs, "Photolithographic olefin metathesis polymerization," J. Am. Chem. Soc. **135**(45), 16817–16820 (2013).
29. S. C. Leguizamon, N. T. Monk, M. T. Hochrein, *et al.*, "Photoinitiated Olefin Metathesis and Stereolithographic Printing of Polydicyclopentadiene," Macromolecules **55**(18), 8273–8282 (2022).
30. A. J. Greenlee, R. A. Weitekamp, J. C. Foster, *et al.*, "PhotoROMP: The Future Is Bright," ACS Catal. **14**(8), 6217–6227 (2024).
31. A. Al Rashid, W. Ahmed, M. Y. Khalid, *et al.*, "Vat photopolymerization of polymers and polymer composites: Processes and applications," Addit. Manuf **47**, 102279 (2021).
32. U. Shaukat, E. Rossegger, and S. Schlögl, "A Review of Multi-Material 3D Printing of Functional Materials via Vat Photopolymerization," Polymers **14**(12), 2449 (2022).
33. A. Bagheri and J. Jin, "Photopolymerization in 3D Printing," ACS Appl. Polym. Mater. **1**(4), 593–611 (2019).
34. Polyspectra, "Print with COR PPE Requirements," https://docs.polyspectra.com/print-cor/ppe-requirements/ (accessed March 25, 2026).
35. R. Bacon, C. Russell, M. Swithenbank, *et al.*, "Free-space terahertz radiation from a LT-GaAs-on-quartz large-area photoconductive emitter," Opt. Express **24**(23), 26986–26997 (2016).
36. J. Neu and C. A. Schmuttenmaer, "Tutorial: An introduction to terahertz time domain spectroscopy (THz-TDS)," J. Appl. Phys. **124**(23), 231101 (2018).
37. B. M. Fischer and P. U. Jepsen, "Dynamic range in terahertz time-domain transmission and reflection spectroscopy," Opt. Lett. **30**(1), 29–31 (2005).
38. P. Kundu, P. Dean, A. Valavanis, *et al.*, "Frequency Tunability and Spectral Control in Terahertz Quantum Cascade Lasers with Phase-Adjusted Finite-Defect-Site Photonic Lattices," IEEE Trans. THz Sci. Technol. **7**(4), 360–367 (2017).
39. D. Mohun, N. Sulollari, M. Salih, *et al.*, "Terahertz microscopy using laser feedback interferometry based on a generalised phase-stepping algorithm," Sci. Rep. **14**(1), 3274 (2024).
40. M. Naftaly and R. E. Miles, "Terahertz time-domain spectroscopy for material characterization," Proc. IEEE **95**(1), 1658–1665 (2007).
41. B. Wen and D. Ban, "High-temperature terahertz quantum cascade lasers," Prog. Quantum Electron. **80**, 100363 (2021).
42. J. Bennett, "Measuring UV Curing Parameters of Commercial Photopolymers used in Additive Manufacturing," Addit. Manuf **18**, 203–212 (2017).
43. L. Phillips, S. Kondawar, H. J. Godden, *et al.*, "Stereolithography 3D Printing of a Cyclic Olefin Resin for Terahertz Quasi-Optical Applications: data," University of Leeds Data Repository, 2026, https://doi.org/10.5518/1791